We are IntechOpen, the world's leading publisher of Open Access books Built by scientists, for scientists

4,800
Open access books available

122,000
International authors and editors

135M
Downloads

Our authors are among the

154
Countries delivered to

TOP 1%
most cited scientists

12.2%
Contributors from top 500 universities

CLARIVATE ANALYTICS BOOK CITATION INDEX INDEXED

WEB OF SCIENCE™

Selection of our books indexed in the Book Citation Index in Web of Science™ Core Collection (BKCI)

Interested in publishing with us?
Contact book.department@intechopen.com

Numbers displayed above are based on latest data collected.
For more information visit www.intechopen.com

Chapter 12

Optimal Locations of Dampers/Actuators in Vibration Control of a Truss-Cored Sandwich Plate

Kongming Guo and Jun Jiang

Additional information is available at the end of the chapter

http://dx.doi.org/10.5772/48615

1. Introduction

In the engineering application of many metal structural components, the damping property is an important factor to be considered. The approaches of adding damping can be mainly divided into two categories: passive vibration control and active vibration control. Passive vibration control with the use of damping materials is widely adopted in the engineering areas due to the simplicity for implementation and the high reliability, while active vibration control using various smart materials as an approach with great potentials has received a great deal of attention in recent years.

A traditional approach to passively suppress vibration of plate-like structure is using constrained layer damping [1] while active vibration control is often realized by bonding piezoelectric patch [2] to the surface of plate. The third approach, semi-active vibration control, adopts piezoelectric switching shunt techniques [3] and active constrained layer damping method [4]. However, the approach should also bond piezoelectric patch or constrained layer to the plate surface. These kinds of techniques are at the expense of adding considerable weight to the structure while the piezoelectric patch cannot generate large enough control force. Moreover, the surface of the plate will be changed. The Kagome sandwich structure [5] introduced in this chapter consists of a solid face sheet, a tetrahedral core and a planar Kagome truss as the back-plane. Because one face sheet of the Kagome structure has been replaced by a planar Kagome truss, the transverse displacement of its solid face sheet can be realized just by the in-plane tension-compression actuation forces if some specific rods in the planar Kagome truss are replaced by linear actuators. This character inspires the design of a new kind of sandwich plate, whose vibration control can be readily realized by replacing a very small portion of the rods only in the planar Kagome truss through cylindrical viscoelastic dampers to dissipate energy or through piezoelectric

stack actuator to generate control forces to suppress the vibration due to the out-of-plane excitation.

It is well known that to keep the expense within the acceptable extent and meanwhile maintain the structure under control, the locations of small number of dampers/actuators used in passive/active vibration control will significantly influence the consequence of the control effect. Determining the optimal locations of dampers/actuators is a combinatory optimization problem since the possible location combinations are discrete. The approaches to achieve an optimal placement of the dampers/actuators can be classified into four categories. The first approach is using ad hoc iterative methods [6] to get the optimal combination, which often obtains the non-optimal solution. The second one solves the discrete problem in a continuous domain [7], which does not provide significant reduction in computational cost. The third method is directly solving the combinatory optimization by using various alternative search techniques like simulated annealing [8] and genetic algorithm [9]. The fourth approach adopts different effectiveness indices, like modal strain energy (MSE) [10] and eigensensitivity [11], to quantify the fitness of different locations. This kind of methods are very intuitive and can often get remarkable results even though they may not be the most optimal ones, while their computational costs are also very low. Moreover, the effectiveness index can help to generate a subset of location combinations that reduces the size of the problem to be dealt with.

This chapter contains three parts: In the first part the Kagome structure and its finite element model is introduced briefly. In the second part passive vibration control of the Kagome structure and optimization of locations of dampers are dealt with. This part is arranged as followings: (1) Building the finite element model of the viscoelastic damper. (2) To control vibration of single mode, fraction of axial MSE is chosen as an effectiveness index to decide the placement position of the dampers in the planar Kagome truss. (3) A practical optimization method of dampers in vibration control of broad-bandwidth vibration control is raised based on MSE. In the third part active vibration control of the Kagome structure and optimization of locations of actuators are discussed. Independent modal space control (IMSC) method is chosen aimed to control the vibration of the lower modes. The third part is arranged as follows: (1) The piezoelectric actuator is introduced. (2) The IMSC method is detailed and its stability is also analyzed. (3) The controllability of IMSC is discussed and an optimization method for the placement of actuators in the Kagome structure that uses both MSE and singular values is developed. (4) The validity of the optimization method is demonstrated through the eigenvalue analysis and the time-domain simulation.

1.1. Kagome sandwich structure

The Kagome based high authority shape morphing structure (or Kagome structure in short) [5] is a kind of sandwich truss-cored plate. In contrast to other sandwich truss-cored plates that have two solid face sheets, one face sheet of the Kagome structure is replaced by a planar Kagome truss while the other face sheet is still a solid one. The truss-core is a tetrahedral truss that lies in between the two faces (see figure 1). The ancient planar Kagome basket weave pattern truss is simultaneously static determinacy and stiff [12]. This feature of

the planar Kagome truss enables its truss rods to be actuated in order to achieve arbitrary in-plane nodal displacements with minimal internal resistance.

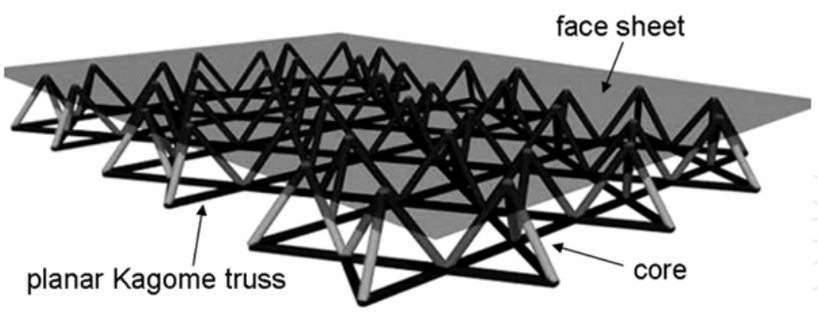

Figure 1. Schematic representation of the Kagome structure, the solid face sheet is shown in dark grey, the core in grey and the planar Kagome truss as one face plane in black.

The material and physical parameters of the Kagome structure studied in this paper are listed in table 1. There are total 1584 truss rods in the planer Kagome truss. Both the solid face sheet and the Kagome back plane of the structure are clamped.

Face sheet		Core truss and Kagome truss	
Material	Al alloy	Material	Stainless steel
Young's modulus	73.1GPa	Young's modulus	193GPa
Density	2700kg/m^3	Density	8030kg/m^3
Length	1.58m	Truss length	51mm
Width	1.50m	Section type	Circle
Depth	1.53mm	Radius	1.275mm

Table 1. Material parameters and size of face sheet and truss rods

MSC.PATRAN is used to build the finite element model of the Kagome structure which is shown in figure 2. The face sheet used is discretized using 1120 plate elements CQUAD4, while the 3167 truss-core and planar Kagome truss is modeled by simple beam elements CBAR. The first six mode shapes are shown in figure 3.

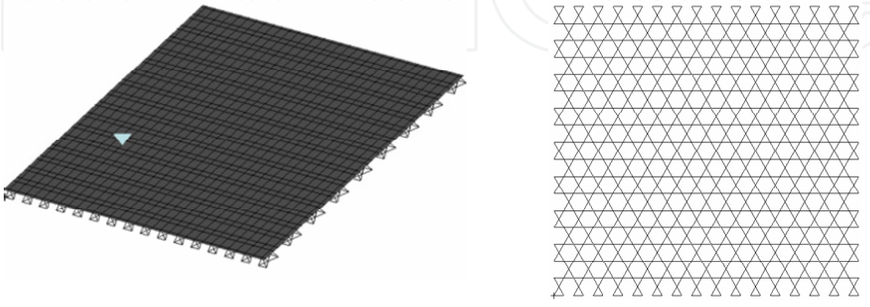

(a) (b)

Figure 2. (a) Finite element model of Kagome structure. The blue triangular represents the observe point of structure response below; (b) The back plane of the Kagome structure with a planar Kagome truss.

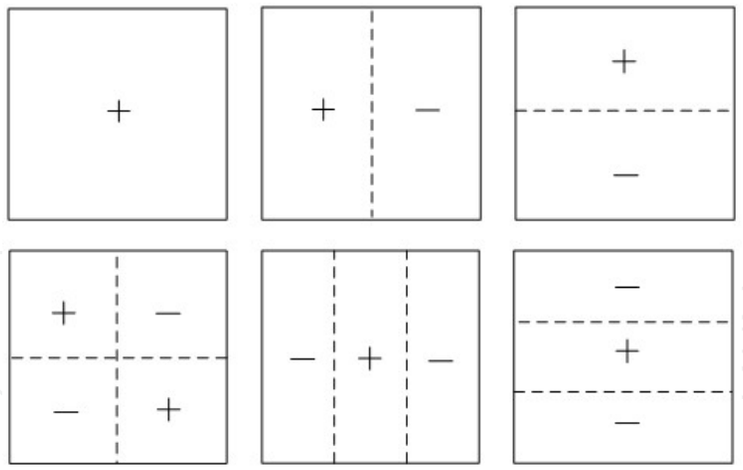

Figure 3. Modal shapes of mode 1-6. The symbol + and – represent the direction of the transverse vibration. The dashed line represents node line.

2. Passive control and damper placement optimization

2.1. Finite element model of viscoelastic damper

According to the feature of the planar Kagome truss, a kind of cylindrical sandwich shearing viscoelastic damper [13] with the same length as the truss members is adopted. This kind of damper is a bi-shearing sandwich structure composed of a core rod, a sleeve and a thin layer of viscoelastic material (see figure 4). When relative movement between the core rod and the sleeve exists, the viscoelastic material will undertake shearing deformation and dissipate energy. To ensure the load applied on the damper in the axial direction, the spherical hinges must be used in the connection between the damper and the truss members in order to avoid bending and torsion moments.

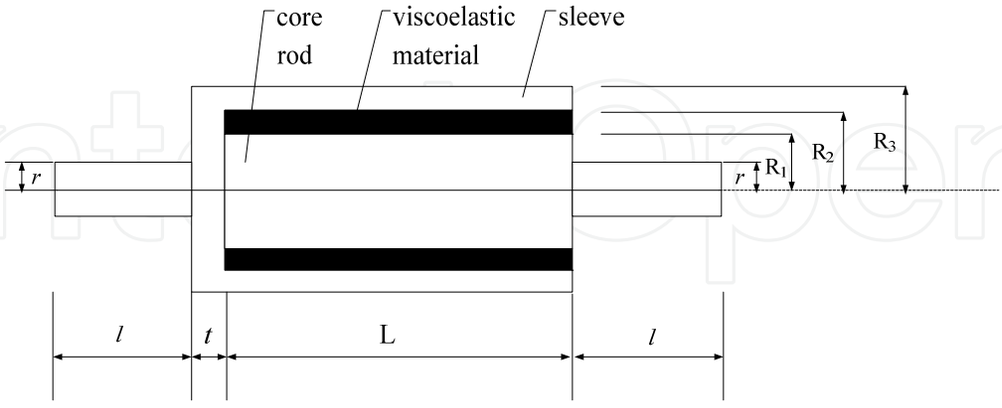

Figure 4. Sketch of the cylindrical sandwich shearing viscoelastic damper. The parameters are given as: L=29mm, t=2mm, l=10mm, r=3mm, R_1=8mm, R_2=10mm, R_3=12.4mm.

To set up a dynamic model of the cylindrical damper which is suitable for the incorporation into the finite element model of the Kagome structure, the theory of linear viscoelasticity is used and the constitutive relation for a viscoelastic material can be written as:

$$\sigma(t) = G(t)\varepsilon(0) + \int_0^t G(t-\tau)\frac{d\varepsilon(\tau)}{d\tau}d\tau \tag{1}$$

where σ is stress and ε represents strain. $G(t)$ is material relaxation function. This stress relaxation represents energy loss from the material. Takeing Laplace transform on (1) yields:

$$\sigma(s) = sG(s)\varepsilon(s) \tag{2}$$

where $sG(s)$ is called material modulus function.

Applying the Biot model [14], the modulus function of viscoelastic material can be written as a series of terms called mini-oscillator terms:

$$sG(s) = G^{\infty}\left(1 + \sum_{k=1}^{m} a_k \frac{s}{s+b_k}\right) \tag{3}$$

The factor G^{∞} represents the equilibrium value of the modulus, $\{a_k, b_k\}$ are positive constant determined by the shape of modulus function in the Laplace domain, $k=1,2,...,m$, while m is the total number of mini-oscillator terms. Figure 5 illustrates the mechanical analogy of Biot model.

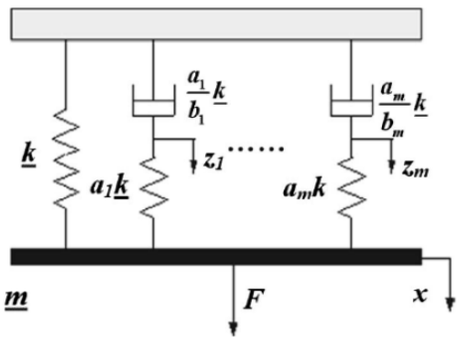

Figure 5. The mechanical analogy of Biot model

The finite element model of the dynamic equation of viscoelastic material by m mini-oscillator terms is written as:

$$\left[\tilde{M}\right]\{\ddot{q}\} + \left[\tilde{C}\right]\{\dot{q}\} + \left[\tilde{K}\right]\{q\} = \{\tilde{f}\} \tag{4}$$

where $q = \{\{x\} \ \{z_1\} \ ... \ \{z_m\}\}^T$ is the variable vector , among it $\{x\}$ represents the displacement vector of the damper, which is governed by the dynamical equation:

$$[M]\{\ddot{x}\} + [K]\left(G(t)\{x(0)\} + \int_0^t G(t-\tau)\{\dot{x}\}d\tau\right) = \{f\} \tag{5}$$

In (5) $[M]$ and $[K]$ are the mass and stiffness matrices of the damper. $\{z_1\},\ldots,\{z_m\}$ are the so-called dissipation coordinates. The symmetric coefficient matrices in (4) are given as:

$$\left[\tilde{M}\right]=\begin{bmatrix}\left[M\right] & \left[0\right] & \cdots & \left[0\right]\\ \left[0\right] & \left[0\right] & \cdots & \left[0\right]\\ \vdots & \vdots & \ddots & \vdots\\ \left[0\right] & \left[0\right] & \cdots & \left[0\right]\end{bmatrix}\left[\tilde{C}\right]=\begin{bmatrix}\left[0\right] & \left[0\right] & \cdots & \left[0\right]\\ \left[0\right] & \dfrac{a_1\left[\bar{\Lambda}\right]}{b_1} & \cdots & \left[0\right]\\ \vdots & \vdots & \ddots & \vdots\\ \left[0\right] & \left[0\right] & \cdots & \dfrac{a_m\left[\bar{\Lambda}\right]}{b_m}\end{bmatrix}\left[\tilde{K}\right]=\begin{bmatrix}\left[K\right](1+\sum_{k=1}^{m}a_k) & -a_1\left[\bar{R}\right] & \cdots & -a_m\left[\bar{R}\right]\\ -a_1\left[\bar{R}\right]^T & a_1\left[\bar{\Lambda}\right] & \cdots & \left[0\right]\\ \vdots & \vdots & \ddots & \vdots\\ -a_m\left[\bar{R}\right]^T & \left[0\right] & \cdots & a_m\left[\bar{\Lambda}\right]\end{bmatrix} \quad (6)$$

with

$$\left[\bar{K}\right]=G^{\infty}\left[K\right]\quad\left[K\right]=\left[R\right]\left[\Lambda\right]\left[R\right]^T\quad\left[\bar{\Lambda}\right]=G^{\infty}\left[\Lambda\right]\quad\left[\bar{R}\right]=G^{\infty}\left[R\right]\left[\Lambda\right]\quad\left\{z\right\}=\left[\bar{R}\right]^T\left\{\hat{z}\right\} \quad (7)$$

where $[\Lambda]$ is a diagonal matrix of the nonzero eigenvalues of matrix $[K]$, and the corresponding normalized eigenvectors form the columns of matrix $[R]$.

The cylindrical damper shown in figure 4 can be regarded as a system with two degrees of freedom. The mass and stiffness matrices in (5) can be defined as:

$$\left[M\right]=\begin{bmatrix}m_c & \\ & m_s\end{bmatrix}\quad\left[K\right]=\frac{G^{\infty}\pi\left(R_1+R_2\right)L}{R_2-R_1}\begin{bmatrix}1 & -1\\ -1 & 1\end{bmatrix}=cG^{\infty}\begin{bmatrix}1 & -1\\ -1 & 1\end{bmatrix} \quad (8)$$

where m_c and m_s are respectively the mass of the core rod and the sleeve. Using equation (7), it can be derived:

$$\bar{\Lambda}=G^{\infty}\Lambda=2cG^{\infty}$$

$$\left[\bar{R}\right]=G^{\infty}\left[R\right]\Lambda=2cG^{\infty}\begin{Bmatrix}\sqrt{2}\\ -\sqrt{2}\end{Bmatrix} \quad (9)$$

So according to (6), the coefficient matrices are:

$$\left[M\right]=\begin{bmatrix}m_c & & & \\ & m_s & & \\ & & 0 & \\ & & & 0\end{bmatrix}\left[C\right]=cG^{\infty}\begin{bmatrix}0 & & & \\ & 0 & & \\ & & \dfrac{2a_1}{b_1} & \\ & & & \dfrac{2a_2}{b_2}\end{bmatrix}\left[K\right]=cG^{\infty}\begin{bmatrix}1+a_1+a_2 & -(1+a_1+a_2) & -a_1\sqrt{2} & -a_2\sqrt{2}\\ -(1+a_1+a_2) & 1+a_1+a_2 & a_1\sqrt{2} & a_2\sqrt{2}\\ -a_1\sqrt{2} & a_1\sqrt{2} & 2a_1 & \\ -a_2\sqrt{2} & a_2\sqrt{2} & & 2a_2\end{bmatrix} \quad (10)$$

We choose ZN-1 rubber as the viscoelastic material, and the parameters of Biot model are fitted as those in table 2:

Parameter	G^{∞}	a_1	a_2	b_1	b_2
Value	5.0013×10^5	2.8438	35.6028	830.1878	13758

Table 2. Fitting parameters of Biot model for ZN-1 at 30℃.

2.2. Vibration control of single mode

Since the rods in the planar Kagome truss are modeled by beam-like elements while the cylindrical dampers can be regarded as a kind of rod element that can not suffer bending and torsion moments, the fraction of axial modal strain energy should be used here. The total modal strain energy of the *i*th mode is written as:

$$E_i = \frac{1}{2}\{\phi\}_i^T [K] \{\phi\}_i \tag{11}$$

where $\{\phi\}_i$ is the mode shape of *i*th mode, and [*K*] is the global stiffness matrix of the structure.

The element *j*'s axial strain energy due to mode *i* is denoted by:

$$E_{ij}^a = \frac{EA}{2L^3}\left(\Delta x_j^1 \Delta\phi_{ij}^1 + \Delta x_j^2 \Delta\phi_{ij}^2 + \Delta x_j^3 \Delta\phi_{ij}^3\right)^2 \tag{12}$$

Here *L* is the length of the truss element. The quantities Δx_j^k, *k=1,2,3* are the components of node coordinate differences of element *j*. $\Delta\phi_{ij}^k$, *k=1,2,3* are the component of node differences in the mode shapes $\{\phi\}_i$ of element *j*. The fraction of axial modal strain energy (FAMSE in short) of element *j* in mode *i* is then define as:

$$\delta_{ij} = \frac{E_{ij}^a}{E_i} \tag{13}$$

This quantity will be used as the effective index to determine which rods are to be replaced by the dampers. Assuming that the damping of the structure is of Rayleigh type and the modal damping ratios of both the first and second modes are 1%, then damping ratios of other modes can be calculated. For modes 1 to 3, we choose 8 rods in the planar Kagome truss, which takes only 0.51% of the total rods in the planar Kagome truss, with significant FAMSE to be replaced by dampers. For the first mode and the second mode, the locations of dampers are the same. The placements of the dampers for every mode are shown in figure 6. It can be seen that the optimal positions of the dampers are all in the constrained boundaries.

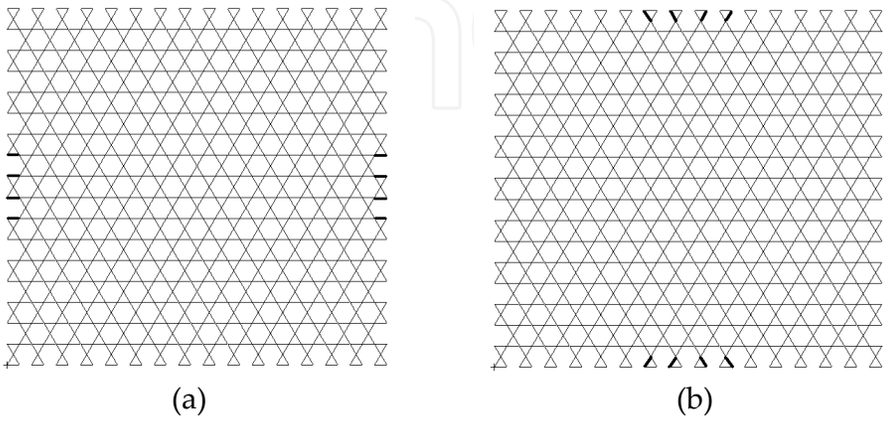

Figure 6. The location of the dampers in the design for different controlled modes. The heavy solid line segments represent the dampers (a) for modes 1 and 2; (b) for mode 3.

The results of complex eigenvalue analysis are listed in table 3 for the vibration control on mode 1 and 2 and in table 4 for the vibration control on mode 3. It is noticed that, because the stiffness of damper is lower than the Kagome truss, the raise of the damping ratio is at the cost of losing stiffness of the structure.

Mode #	Damping ratio	Increment of damping ratio	Frequency(Hz)	Decrement of frequency(%)
1	0.0300	0.0200	112	5.08
2	0.0311	0.0211	208	4.59
3	0.0118	0.0016	231	0.43

Table 3. The result of complex modal analysis under the dampers placement design for mode 1&2.

Mode #	Damping ratio	Increment of damping ratio	Frequency(Hz)	Decrement of frequency(%)
1	0.0243	0.0143	113	4.24
2	0.0104	0.0004	217	0.46
3	0.0309	0.0207	222	4.31

Table 4. The result of complex modal analysis under the dampers placement design for mode 3.

2.3. Broad-bandwidth vibration control

In practice, the structure often suffers excitation with broad-bandwidth frequency, so a control method which can suppress the vibration of several modes is introduced below. Here FAMSE is continuously used as an index to optimize the location of the dampers. The target is to search the truss elements with remarkably large FAMSE among all the target modes. According to the excitation frequency band in the case studied here, the target modes are chosen to be the first six modes. In this paper the number of dampers used is 20, which takes only 1.26% of total rods in the planar Kagome truss.

The total FAMSE in mode i of the N=20 chosen elements (rods) is defined as:

$$\delta_i = \sum_{j}^{20} \delta_{ij},\ i = 1,...6 \tag{14}$$

Let e=minδ_i (i varies from *1* to *6*) indicate the minimum of total FAMSE from mode 1 to mode 6 for the *20* chosen elements. The target of the optimization is to maximize e by selecting different combination of *20* elements. To simplify the optimization procedure, total FAMSE of all the six modes in element j is defined as:

$$\delta_j = \sum_{i}^{6} \delta_{ij}. \tag{15}$$

In the optimization procedure, 100 elements that have the top largest δ_j are first determined from 1584 truss rods. Then, 20 elements will be selected from the 100 elements. Assuming

the placement of the dampers is symmetrical, and the computation of the optimization search can get further reduction. As above, the optimal positions of the dampers are in the constrained boundaries (see figure 7(a)). For the purpose of comparison, the dampers are also placed in a relatively uniform style as shown by figure 7(b).

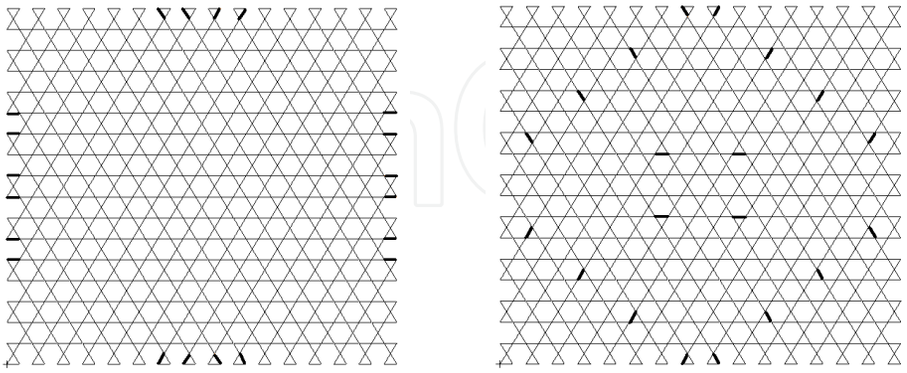

(a) (b)

Figure 7. (a) The position of the dampers using FAMSE method; (b) The positions of the dampers in a relatively uniform style. The heavy solid line segments represent the dampers.

Mode#	Damping ratio	Increment of damping ratio	Frequency(Hz)	Decrement of frequency(%)
1	0.0460	0.0360	106	10.17
2	0.0329	0.0229	207	5.05
3	0.0382	0.0281	218	6.03
4	0.0260	0.0141	310	2.52
5	0.0365	0.0237	343	3.65
6	0.0321	0.0186	376	3.34

(a)

Mode#	Damping ratio	Increment of damping ratio	Frequency(Hz)	Decrement of frequency(%)
1	0.0243	0.0143	104	11.86
2	0.0201	0.0101	201	7.80
3	0.0226	0.0124	211	9.05
4	0.0235	0.0116	285	10.38
5	0.0258	0.0130	323	9.27
6	0.0248	0.0113	358	7.97

(b)

Table 5. The results of complex modal analysis with the dampers.(a) placement of dampers using FAMSE method; (b) Placement of dampers in a relatively uniform style.

The results of the damping ratios and the natural frequencies of the Kagome structure with dampers through complex eigenvalue analysis are shown table 5. It can be seen that the damping ratios of mode 1 to 6 have been considerably increased. The optimized placement

of the dampers using FAMSE method achieves better results in comparison with those by a relatively uniform placement of the dampers (compare data in table 5(a) and 5(b)). Beside the smaller increment of damping ratios, the stiffness of the Kagome structure is significantly reduced as shown by the sharp decrease of natural frequencies of all six modes.

To validate this passive vibration control method, responses of the Kagome structure during the excitation of vertically downward distributed white noise load on the solid face sheet are computed. The noise is with finite bandwidth of 2000Hz. The single-side power spectrum density is $10N^2/Hz$.

The lateral responses of the Kagome structure, observed at the point shown in figure 2(a), in the cases without dampers, with the dampers in placement as shown in figure 7(a) and in figure 7(b) are drawn in figure 8. It is found that the response amplitudes are considerably reduced with the installation of the dampers in the structure. The response amplitudes in the case with optimized placement of the dampers are even smaller than those in the case of the relatively uniform placement of the dampers.

From the spectra of the responses shown in figure 8(b), the effectiveness of the passive vibration control method proposed in this paper can be easily seen. The advantage of the optimal placement of the dampers over the relatively uniform placement of the dampers can also be observed. Furthermore, due to decrease of stiffness, the shift of the resonance peaks is detectable.

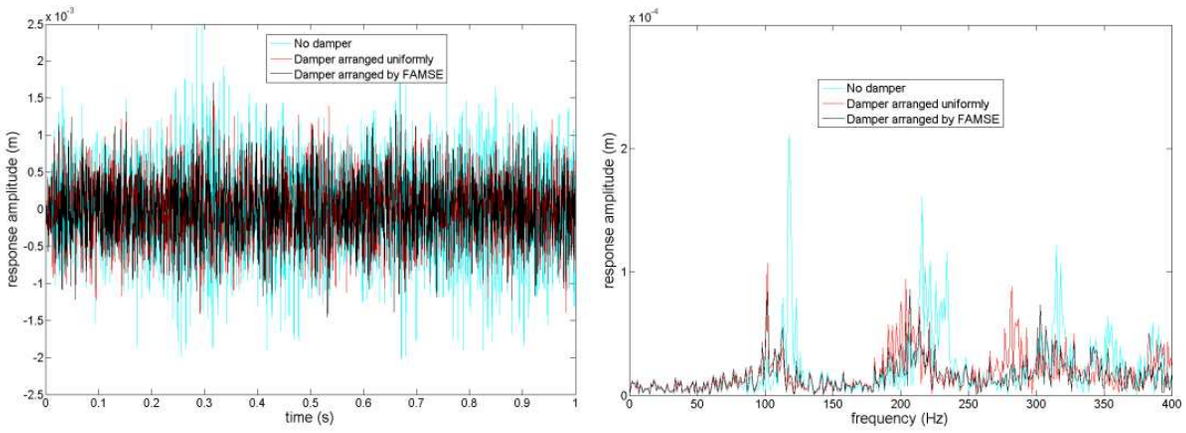

(a) (b)

Figure 8. (a) The time history of response under the excitation of white noise; (b) Spectra of responses.

3. Active vibration control

3.1. Piezoelectric actuator

To realize active control, a rod-like piezoelectric actuators are adopted (see figure 9) to replace small number of rods in the planar Kagome truss of the Kagome structure. The actuator is mainly composed of a piezoelectric stack, outer casing, preloading spring and two link rods. A sphere joint is used to prevent the piezoelectric stack from bending and torsion moments.

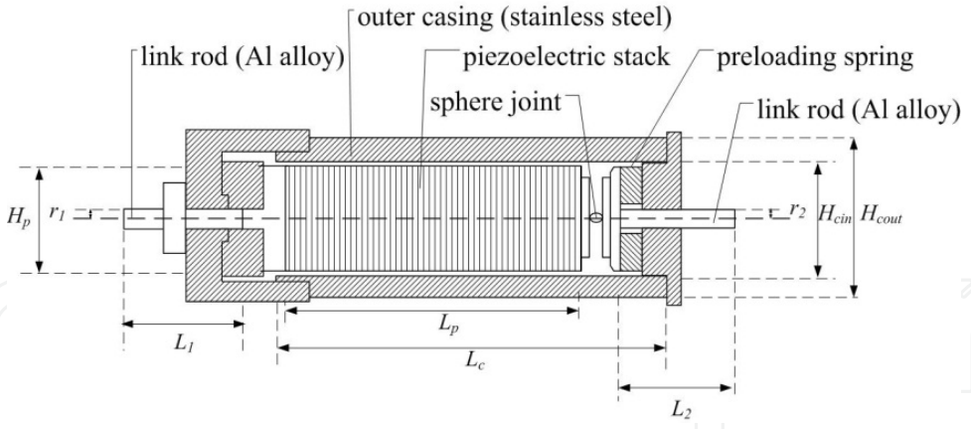

Figure 9. Sketch of the piezoelectric actuator. The parameters are given as: L_1=L_2=8mm, L_p=30mm, L_c=40mm, H_p=10mm, r_1=r_2=1.3mm, H_{cin}=12mm, H_{cout}=15mm.

After combining the finite element model of the two link rods with piezoelectric stack and condensing the internal degrees of freedom in two connected points, the finite element model of the actuator in its local coordinate can be written as:

$$\left[M^{\mathrm{e}}\right]\left\{\ddot{q}^{\mathrm{e}}\right\}+\left[K^{\mathrm{e}}\right]\left\{q^{\mathrm{e}}\right\}=\left\{f^{\mathrm{e}}\right\}-\left[K_{\mathrm{c}}^{\mathrm{e}}\right]\phi \tag{16}$$

where $[M^e]$ is the mass matrix, $[K^e]$ the stiffness matrix, $[K_c^e]$ the coupling matrix connecting the mechanical variables $\{q^e\}$and the electrical variables ϕ. The matrices are in the following forms [15]:

$$\left[M^{\mathrm{e}}\right]=\begin{bmatrix}\frac{1}{2}m_{\mathrm{p}}+m_1 & \\ & \frac{1}{2}m_{\mathrm{p}}+m_3+m_{\mathrm{t}}\end{bmatrix}\quad\left[K^{\mathrm{e}}\right]=\frac{k_1k_2k_3}{k_1k_2+k_2k_3+k_1k_3}\begin{bmatrix}1 & -1\\ -1 & 1\end{bmatrix}\quad\left[K_{\mathrm{c}}^{\mathrm{e}}\right]=nd_{33}k_2\begin{bmatrix}-1\\ 1\end{bmatrix} \tag{17}$$

Here m_p ,m_1, m_3 are masses of piezoelectric stack and two link rods respectively, and m_t is the total mass of outer casing and spring. The masses of other components are ignored. k_1 and k_3 are the stiffness of the two link rods while k_2 is the equivalent stiffness of the piezoelectric stack, the outer casing and the spring. n is the number of disks in the stack and piezoelectric strain constant d_{33} means induced strain in axial direction of the stack per unit electric field applied in axial direction. Under the designed size, the actuator can match the truss rod both in length and in axial stiffness. Choose actuate voltage V= $-\phi$, the control force of the actuator is given by:

$$u^{\mathrm{e}}=nd_{33}k_2V \tag{18}$$

3.2. Independent modal space control

After incorporating the actuator model into the Kagome structure, the global dynamic equations of the actuated Kagome structure without excitation could be written as:

$$\begin{aligned}
&\left[M\right]\left\{\ddot{q}\right\}+\left[D\right]\left\{\dot{q}\right\}+\left[K\right]\left\{q\right\}=\left[B_{\mathrm{s}}\right]\left\{u\right\}\\
&\left\{y_{\mathrm{d}}\right\}=\left[C_{\mathrm{d}}\right]\left\{q\right\}\\
&\left\{y_{\mathrm{v}}\right\}=\left[C_{\mathrm{v}}\right]\left\{\dot{q}\right\}
\end{aligned} \tag{19}$$

where $\{q\}$,$\{\dot{q}\}$ and $\{\ddot{q}\}$ are the N-length vectors of displacement, velocity and acceleration, respectively , with N being the degree of freedoms of the structure. [M], [D] and [K] are $N\times N$ mass, damping and stiffness matrices, respectively. [B_{s}] is $N\times s$ spatial coupling matrix relative to the s-length physical control force vector {u}. The r-length output vectors {y_{d}}and {y_{v}} are related to the displacement and velocity vectors through the matrices [C_{d}] and [C_{v}], respectively. s is the number of actuators while r is number of sensors. In IMSC method (see below), r and s equal the number of modes to be controlled.

In structure vibration, the lower modes often possess the most energy and play more critical roles. Meirovitch [16] developed an independent modal space control (IMSC) method aimed to control the vibration of the lower modes. In IMSC, the dynamic equation of structure is decoupled using modal analysis and then modal control forces are determined by various control laws. The design of control law and the placement of actuators are two independent steps in IMSC.

In IMSC, the modes are divided into two parts: controlled modes and residual modes. In what follows, the subscripts c and r will refer to the controlled and the residual modes respectively.

Assume that [ψ] is the modal matrix composed of the controlled modes [ψ_{c}] and residual modes [ψ_{r}]. Let:

$$\left\{q\right\}=\left[\Psi\right]\left\{q_{\mathrm{m}}\right\}=\left[\Psi_{\mathrm{c}}\right]\left\{q_{\mathrm{mc}}\right\}+\left[\Psi_{\mathrm{r}}\right]\left\{q_{\mathrm{mr}}\right\} \tag{20}$$

where {q_{m}} is the vector of modal displacement consists of the controlled part {q_{mc}} and the residual part {q_{mr}}. Substitute (20) into (19), and left multiple the first equation of (19) by [ψ]$^{\mathrm{T}}$ to yield:

$$\begin{aligned}
&\begin{Bmatrix}\ddot{q}_{\mathrm{mc}}\\ \ddot{q}_{\mathrm{mr}}\end{Bmatrix}+\left[D_{\mathrm{d}}\right]\begin{Bmatrix}\dot{q}_{\mathrm{mc}}\\ \dot{q}_{\mathrm{mr}}\end{Bmatrix}+\left[\Lambda\right]\begin{Bmatrix}q_{\mathrm{mc}}\\ q_{\mathrm{mr}}\end{Bmatrix}=\begin{bmatrix}\left[B_{\mathrm{mc}}\right]\\ \left[B_{\mathrm{mr}}\right]\end{bmatrix}\left\{u\right\}\\
&\left\{y_{\mathrm{d}}\right\}=\left[C_{\mathrm{dmc}}\right]\left\{q_{\mathrm{mc}}\right\}+\left[C_{\mathrm{dmr}}\right]\left\{q_{\mathrm{mr}}\right\}\\
&\left\{y_{\mathrm{v}}\right\}=\left[C_{\mathrm{vmc}}\right]\left\{\dot{q}_{\mathrm{mc}}\right\}+\left[C_{\mathrm{vmr}}\right]\left\{\dot{q}_{\mathrm{mr}}\right\}
\end{aligned} \tag{21}$$

where [D_{d}]=*diag*($2\xi_i\omega_i$), [Λ]=*diag*(ω_i^2), [B_{mc}]= [ψ_{c}]$^{\mathrm{T}}\times$[B_{s}] , [B_{mr}]= [ψ_{r}]$^{\mathrm{T}}\times$[B_{s}] , [C_{dmc}]=[C_{d}]$\times$[ψ_{c}] , [C_{dmr}]=[C_{d}]$\times$[ψ_{r}] , [C_{vmc}]= [C_{v}]$\times$[ψ_{c}] , [C_{vmr}]= [C_{v}]$\times$[ψ_{r}], ξ_i and ω_i are the damping ratio and the circle frequency of mode i. Define the modal control forces of the controlled modes as:

$$\left\{f_{\mathrm{c}}\right\}=\left[B_{\mathrm{mc}}\right]\left\{u\right\} \tag{22}$$

and the equation of the controlled modes can be written as:

$$\{\ddot{q}_{\mathrm{mc}}\}+[D_{\mathrm{dc}}]\{\dot{q}_{\mathrm{mc}}\}+[\Lambda_{\mathrm{c}}]\{q_{\mathrm{mc}}\}=\{f_{\mathrm{c}}\} \tag{23}$$

where $[\Lambda_{\mathrm{c}}]$ and $[D_{\mathrm{dc}}]$ are diagonal matrices like $[\Lambda]$ and $[D_{\mathrm{d}}]$ but only contain the elements corresponding to the controlled modes.

In IMSC, the modal control force vector $\{f_{\mathrm{c}}\}$ is first determined then physical control force vector $\{u\}$ will be calculated from $\{f_{\mathrm{c}}\}$. Equation (23) consists of n independent equations for each of the controlled mode. For the ith mode the equation is given as:

$$\ddot{q}_i+2\xi_i\omega_i\dot{q}_i+\omega_i^2q_i=f_i \tag{24}$$

when modal displacement and velocity are obtained, the control force will be taken in the form:

$$f_i=-[G_i]\{q_i \quad \dot{q}_i\}^{\mathrm{T}} \tag{25}$$

The modal velocity feedback control will be adopted:

$$[G_i]=[0 \quad 2\omega_i(\xi_{ic}-\xi_i)]=[0 \quad g_{vi}] \tag{26}$$

while ξ_{ic} is the designed damping ratio of mode i. If modal control force $\{f_{\mathrm{c}}\}$ is determined, the physical control force vector $\{u\}$ can be calculated by using:

$$\{u\}=[B_{\mathrm{mc}}]^{-1}\{f_{\mathrm{c}}\} \tag{27}$$

In general, the modal states in (25) are not directly available. So an observer is needed to reconstruct the modal states from the physical signals measured by sensors. To do so, the part of equation (21) which governs the controlled modes is reformulated in state-space form as:

$$\begin{aligned}\{\dot{x}_{\mathrm{c}}\}&=[A_{\mathrm{c}}]\{x_{\mathrm{c}}\}+[B_c]\{u\}\\ \{y_{\mathrm{c}}\}&=[C_{\mathrm{c}}]\{x_{\mathrm{c}}\}\end{aligned} \tag{28}$$

where $[A_{\mathrm{c}}]$ is $2n\times 2n$ system matrix, $[B_{\mathrm{c}}]$ is $2n\times n$ input matrix and $[C_{\mathrm{c}}]$ is $n\times 2n$ output matrix in the following forms:

$$\{x_{\mathrm{c}}\}=\{\{q_{\mathrm{mc}}\} \quad \{\dot{q}_{\mathrm{mc}}\}\}^{\mathrm{T}} \quad [A_c]=\begin{bmatrix}0 & [I]\\ -[\Lambda_{\mathrm{c}}] & -[D_{\mathrm{dc}}]\end{bmatrix} \quad [B_{\mathrm{c}}]=\begin{bmatrix}[0]\\ [B_{\mathrm{mc}}]\end{bmatrix} \quad [C_{\mathrm{c}}]=\begin{bmatrix}[C_{\mathrm{dmc}}] & 0\\ 0 & [C_{\mathrm{dvc}}]\end{bmatrix} \tag{29}$$

with $[I]$ being the identity matrix. The modal control force vector in state space can be written as:

$$\{F_c\}=-[G]\{x_{\mathrm{c}}\} \tag{30}$$

where

$$[G]=\begin{bmatrix} 0 & 0 & \cdots & 0 & g_{v1} & 0 & \cdots & 0 \\ 0 & 0 & \cdots & 0 & 0 & g_{v2} & \cdots & 0 \\ \vdots & \vdots & \ddots & \vdots & \vdots & \vdots & \ddots & \vdots \\ 0 & 0 & \cdots & 0 & 0 & 0 & \cdots & g_{vn} \end{bmatrix} \tag{31}$$

Since modal states are not directly available, the estimated modal states $\{\hat{x}_c\}$ will be used instead, so $\{F_c\}$ is rewritten as:

$$\{F_c\}=-[G]\{\hat{x}_c\} \tag{32}$$

To get the estimated modal states from the measured signals, an observer, e.g., Kalman filter, is adopted in this paper to identify the modal displacements and velocities. The Kalman filter dynamics can be described as:

$$\{\dot{\hat{x}}_c\}=[A_c]\{\hat{x}_c\}+[B_c]\{u\}+[H_c](\{y_c\}-[C_c]\{\hat{x}_c\}) \tag{33}$$

The observer gain matrix $[H_c]$ may be determined by solving the following Riccati equation:

$$[P][A_c]^T+[A_c][P]-[P][C_c]^T[V]^{-1}[C_c][P]+[W]=0 \tag{34}$$

where $[P]$ is the solution, while $[W]$ and $[V]$ are, respectively, the covariance intensity matrices of process and measurement noises. The observer gain $[H_c]$ is obtained from:

$$[H_c]=[P][C_c]^T[V]^{-1} \tag{35}$$

Since IMSC uses the reduced model, the situation may occur that the damping ratios of the controlled modes increase while the damping ratios of the residual modes may decrease (spillover). When the damping ratio of any residual modes drops below zero, the controlled system will become instable. To analyze the stability of the controlled system, the governing equation of the whole system with control will be developed. To get the equation of the whole system, the equations of residual modes in state-space is obtained as that in (28). Now the equations of the system with the observer for ISMC can be written as:

$$\begin{aligned} \{\dot{x}_c\}&=[A_c]\{x_c\}+[B_c]\{u\} \\ \{\dot{x}_r\}&=[A_r]\{x_r\}+[B_r]\{u\} \\ \{y_c\}&=[C_c]\{x_c\} \\ \{\dot{\hat{x}}_c\}&=[A_c]\{\hat{x}_c\}+[B_c]\{u\}+[H_c](\{y_c\}-[C_c]\{\hat{x}_c\}) \end{aligned} \tag{36}$$

To analyze the stability of the controlled system, the observer error vector, $\{e_c\}=\{x_c\}-\{\hat{x}_c\}$, is defined, and the governing equation is rewritten in the matrix form as:

$$\begin{pmatrix} \{\dot{x}_c\} \\ \{\dot{x}_r\} \\ \{\dot{e}_c\} \end{pmatrix} = \begin{pmatrix} [A_c]-[B_c^*][G] & 0 & [B_c^*][G] \\ -[B_r^*][G] & [A_r] & [B_r^*][G] \\ 0 & -[H_c][C_r] & [A_c]-[H_c][C_c] \end{pmatrix} \begin{pmatrix} \{x_c\} \\ \{x_r\} \\ \{e_c\} \end{pmatrix} \tag{37}$$

where

$$[B_c^*] = \begin{bmatrix} 0 \\ [I] \end{bmatrix} \quad [B_r^*] = \begin{bmatrix} 0 \\ [B_{mr}][B_{mc}]^{-1} \end{bmatrix} \tag{38}$$

The controlled system is stable when all the eigenvalues of system matrix have negative real parts. The term $[H_c][C_r]$ contaminates the sensor output by the residual modes, known as observation spillover. Meanwhile, the residual modes are excited via the term $[B^*_r][G]$ called control spillover. Spillover can make residual modes unstable, that is, the eigenvalues corresponding to these modes will have positive real parts. Since the control spillover solely has no effect on the eigenvalues of the controlled system, spillover can be avoided when the observation spillover is suppressed. To alleviate the observation spillover, equations (34) and (35) will be rewritten in the form [17]:

$$\begin{aligned} &[P][A_c]^T + [A_c][P] - [P][C_c]^T[\tilde{V}]^{-1}[C_c][P] + [W] = 0 \\ &[H_c] = [P][C_c]^T[\tilde{V}]^{-1} \end{aligned} \tag{39}$$

where:

$$[\tilde{V}] = [V] + [C_r][V_1][C_r]^T \tag{40}$$

$[V_1]$ is a weighting matrix which allows to desensitize the estimated states to the residual modes. The block diagram of the controlled system is shown in figure 10:

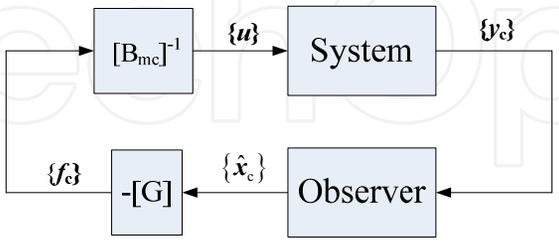

Figure 10. The block diagram of close-loop system.

3.3. Actuator placement optimization in ISMC method

For the placement of actuators in IMSC, Baruh [18] pointed out that the energy going into the controlled modes is independent of the actuator locations but the energy pumped into the uncontrolled modes depends on the actuator locations. Lindberg Jr [19] indicated that

improperly chosen locations can make the actuator forces grow to infinity, that is, the system became uncontrollable. So the singular values of input matrix can be used to optimize the actuator locations in order to reduce the control effort and suppress spillover. Lammering [20] used the trace of the input matrix as the objective function to minimize the control energy and spillover, while electric potentials (something like MSE) was introduced as an effectiveness index to get a subset of suitable locations.

3.3.1. Objective function for optimization

From (26) it is known that the system is controllable if and only if $[B_{mc}]$ is of full rank. Otherwise, the modal control forces can not be realized physically. It is also known that the goal of actuator optimization is not just simply to meet the condition of controllability. The extent of controllability that can provide a quantitative measurement on the physical actuator force vector needed for a given modal control force vector is also of great interest [21]. For a modal control force vector designed to achieve the expected control effect, it is highly expected that through actuator placement optimization, smaller physical control forces will be required to realize a more controllable system. Of course, the physical control forces will grow to infinity if the system is uncontrollable.

Lammering [20] proposed an optimization method for the actuator placement by using the trace of matrix $\left(\left[B_{\mathrm{mc}}\right]^{\mathrm{T}}\right)^{-1}\left[B_{\mathrm{mc}}\right]^{-1}$ as the criterion in order to make the total control effort, i.e., the square of the norm of the physical control force $\{u\}^{\mathrm{T}}\{u\}$ to become minimum. The corresponding objective function is thus given by:

$$tr\left(\left(\left[B_{\mathrm{mc}}\right]^{\mathrm{T}}\right)^{-1}\left[B_{\mathrm{mc}}\right]^{-1}\right)\rightarrow \min \tag{41}$$

Different from the above method, the minimization of the maximal physical control force will be the objective in the present paper. Meanwhile, the singular values of the input matrix $[B_{mc}]$ are used to measure the controllability.

The singular value decomposition of input matrix $[B_{mc}]$ is done as the following:

$$\left[B_{\mathrm{mc}}\right]_{n\times n}=\left[U\right]_{n\times n}\left[S\right]_{n\times n}\left[Q\right]_{n\times n} \tag{42}$$

with $[U]^{\mathrm{T}}[U]= [Q]^{\mathrm{T}}[Q]=[I]$, $\left[S\right]=\begin{bmatrix}\left[\Sigma\right] & 0\\ 0 & 0\end{bmatrix}$ and $[\sum]=\mathrm{diag}[\sigma_1, \sigma_2,\ldots, \sigma_m]$, where σ_i is the ith singular value of $[S]$. Here assume the system is controllable, so $[B_{mc}]$ and $[S]$ are of full rank, and $[S] = [\sum]$.

To illustrate the relationship among modal control forces, singular values and physical control forces, we introduce a new modal coordinate $\{\eta\}$ through the coordinate transformation [21]:

$$\{q\} = [\psi][U]\{\eta\} = [\psi^*]\{\eta\} \tag{43}$$

where $[\psi^*]$ is also a modal matrix of the system which obviously satisfies the orthogonality condition with respect to the mass matrix $[M]$. Obviously $\{\eta\}$ can also be divided into the controlled modes $\{\eta_c\}$ and the residual modes $\{\eta_r\}$. Since the dynamical equation is decoupled in the modal coordinates, only the controlled part will be considered below. By substituting (43) into (19) a new form of equation governing the controlled modes can be obtained as:

$$\{\ddot{\eta}_c\} + [D_{dc}]\{\dot{\eta}_c\} + [\Lambda_c]\{\eta_c\} = [S]\{u^*\} \tag{44}$$

with $\{u^*\} = [Q]^T\{u\}$. Because $[Q]^T[Q]=[I]$, $\{u^*\}$and $\{u\}$ can be considered to be equivalence. Denote the right part of equation (44) as:

$$\{f_c^*\} = [S]\{u^*\} \tag{45}$$

Of course $\{f_c^*\}$ is still the modal control force. From (45) the follow relation between the modal control force $\{f_c^*\}$ and physical control force $\{u^*\}$ can be derived as:

$$\{u^*\} = [S]^{-1}\{f_c^*\} = diag[1/\sigma_1 \quad 1/\sigma_2 \quad \cdots \quad 1/\sigma_n]\{f_c^*\} \tag{46}$$

The relationship between the ith element of $\{u^*\}$ and $\{f_c^*\}$ is:

$$u_i^* = f_{ci}^*/\sigma_i \tag{47}$$

Here it is supposed that the elements in $\{f_c^*\}$ are within the same fixed range, which is supposed from $-b$ to $+b$. The maximal value u^*_{max} in $\{u^*\}$, on the other hand, will be:

$$\left|u_{max}^*\right| = b/\sigma_{min} \tag{48}$$

In this way, the amplitude of maximal element in $\{u^*\}$ depends on the minimal singular value σ_{min} of $[B_{mc}]$. If the minimal singular value of $[B_{mc}]$ is larger, the maximal physical control force will be smaller. So the optimization objective function becomes:

$$\sigma([B_{mc}])\big|_{min} \rightarrow \max \tag{49}$$

3.3.2. Selection of candidate locations though modal strain energy

The computational cost of optimization may become too high to be affordable if all the combinations are calculated in order to find the most optimal combination that meets criterion (49). However, the computational cost of optimization can be significantly reduced when a proper subset of combinations may be first defined. In this part, FAMSE will also be

used as the index to determine the subset. And it will be shown below that MSE solely can not properly determine the locations of actuators in the present case.

To investigate the suitability of FAMSE in IMSC method, the case to control one mode vibration is first studied. According to IMSC method, only one actuator is needed in the case, the input matrix [B_{mc}] now has only one element denoted by:

$$B_{\mathrm{mc}} = \left\{\psi_i\right\}^{\mathrm{T}} \left[B_{\mathrm{s}}\right] = \frac{\Delta x_j^1 \Delta\phi_{ij}^1 + \Delta x_j^2 \Delta\phi_{ij}^2 + \Delta x_j^3 \Delta\phi_{ij}^3}{L} \tag{50}$$

while the axial MSE of the element j for the controlled mode i is given by:

$$E_{ij}^{\mathrm{a}} = \frac{EA}{2L^3}\left(\Delta x_j^1 \Delta\phi_{ij}^1 + \Delta x_j^2 \Delta\phi_{ij}^2 + \Delta x_j^3 \Delta\phi_{ij}^3\right)^2 = \frac{EA}{2L}\left(B_{\mathrm{mc}}\right)^2 \tag{51}$$

Assume B_{mc} is positive, the relationship between B_{mc} and axial MSE is:

$$B_{\mathrm{mc}} = \sqrt{\frac{2L}{EA} E_{ij}^{\mathrm{a}}} \tag{52}$$

So according to the magnitude of the value E_{ij}^{a}, the most proper location of the actuator can be chosen, that is, the axial MSE can work as an index for the actuator placement in the case.

Let us now examine the case of vibration control on multiple modes. Assume that the number of modes to be controlled is n by using the same number of actuators. The input matrix [B_{mc}] is in the form:

$$\left[B_{\mathrm{mc}}\right] = \sqrt{\frac{2L}{EA}} \begin{bmatrix} \pm\sqrt{E_{11}^{\mathrm{a}}} & \pm\sqrt{E_{12}^{\mathrm{a}}} & \cdots & \pm\sqrt{E_{1n}^{\mathrm{a}}} \\ \pm\sqrt{E_{21}^{\mathrm{a}}} & \pm\sqrt{E_{22}^{\mathrm{a}}} & \cdots & \pm\sqrt{E_{2n}^{\mathrm{a}}} \\ \vdots & \vdots & \ddots & \vdots \\ \pm\sqrt{E_{n1}^{\mathrm{a}}} & \pm\sqrt{E_{n2}^{\mathrm{a}}} & \cdots & \pm\sqrt{E_{nn}^{\mathrm{a}}} \end{bmatrix} \tag{53}$$

where the signs of the elements in each row of the input matrix are determined according to the corresponding mode shape.

Below, through two simple examples, it will be demonstrated that if the locations of actuators are optimized just in accordance to the magnitudes of the values of axial MSE in the Kagome structure, the controllability of the system, or the condition of the full rank of the corresponding input matrix [B_{mc}], can not be guaranteed. Let us investigate the control of the vibration accounting for the second and the third modes of the Kagome structure with two actuators by using IMSC. In figure 11, two kinds of placement of actuators are shown. It is noted that even though the axial MSE of the elements in the positions of the actuators are of the equal values for each mode due to the symmetry of the structure, the rank of the input matrix [B_{mc}] differs greatly in the two cases.

In case (a) of figure 11, the input matrix has the form:

$$\left[B_{\mathrm{mc}}\right]=\sqrt{\frac{2L}{EA}}\begin{pmatrix}-\sqrt{E_{21}^{\mathrm{a}}} & \sqrt{E_{22}^{\mathrm{a}}}\\ -\sqrt{E_{31}^{\mathrm{a}}} & \sqrt{E_{32}^{\mathrm{a}}}\end{pmatrix}=\begin{pmatrix}-0.0134 & 0.0134\\ -0.0137 & 0.0137\end{pmatrix} \tag{54}$$

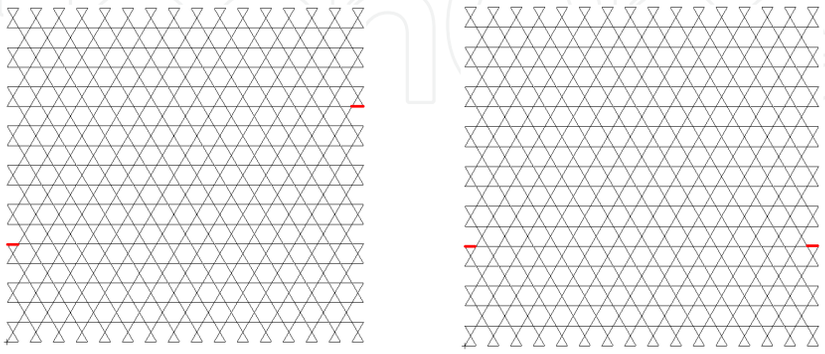

(a) (b)

Figure 11. Different locations of the actuators on the planar Kagome used to control mode 2 and 3. The heavy red line segments represent the actuators.

It is obvious that the matrix $[B_{mc}]$ is singular and the system becomes uncontrollable. Similar phenomenon was also found in [20]. On the other hand, the input matrix for case (b) in figure 11 is in the form:

$$\left[B_{\mathrm{mc}}\right]=\sqrt{\frac{2L}{EA}}\begin{pmatrix}-\sqrt{E_{21}^{\mathrm{a}}} & \sqrt{E_{22}^{\mathrm{a}}}\\ -\sqrt{E_{31}^{\mathrm{a}}} & -\sqrt{E_{32}^{\mathrm{a}}}\end{pmatrix}=\begin{pmatrix}-0.0134 & 0.0134\\ -0.0137 & -0.0137\end{pmatrix} \tag{55}$$

which is in full rank.

By examining the mode shapes of mode 2 and 3 as given in figure 3, it is seen that in case (a), the two actuators are in the locations of anti-phase for both of the two modes, while in case (b), the two actuators are in the positions of anti-phase for mode 2 but in the positions of in-phase for mode 3. So the consequence of the actuator placement on the effect of control is also close related to the mode shapes of the modes to be controlled beside the values of axial MSE.

3.3.3. A two-step optimization method

Based on above analysis, a two-step optimization method for the placement of actuators in the Kagome structure is proposed as follows:

Step 1. Denote the collection of N_i elements which contains the elements in the planar Kagome with the largest axial MSE of mode i by $\{U_i\}=\{ele_{1i},ele_{2i},\ldots,ele_{Ni}\}$. Since one

actuator is used by IMSC method, an element is chosen from the subset $\{U_i\}$ for the control of mode i. When the total number of modes to be controlled is n, the number of candidate sets of actuator locations is $(N_i)^n$. Due to the existence of repeated elements in different $\{U_i\}$, the actual number is always less than $(N_i)^n$.

Step 2. Calculate the singular-values of the input matrix $[B_{mc}]$ of all the combinations, and the optimal combination should be the one that meet the objective function (49).

3.4. Numerical simulations

In this chapter the vibration control on the Kagome structure covering the bandwidth of the first six modes will be implemented. According to IMSC method, six actuators and six sensors are needed. Here, the accelerometers are used as sensors to measure the z-direction (out-of-plane) acceleration of the Kagome planar truss and the information of displacement and velocity can be derived through integration. The placement of sensors is determined by choosing the nodes where the peak of the mode shape of mode i, $i=1\sim6$, locates. The positions of sensors are shown in figure 12.

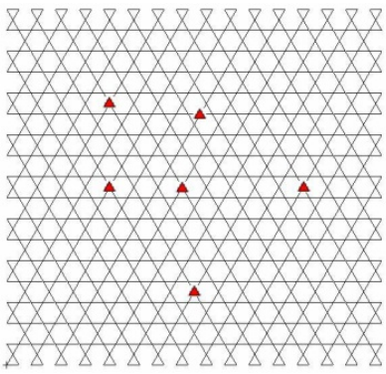

Figure 12. Locations of accelerometers in the planar Kagome (red triangles).

To obtain the optimal actuator locations, 12 elements in the planar Kagome of the Kagome structure which have the largest axial MSE in mode i are selected to form the subset $\{U_i\}$ (i=1~6). By using the two-step optimization method above, the optimized locations of actuators are obtained as shown in figure 13(a). For the purpose of comparison, the non-optimal locations of actuators chosen just in accordance with the same MSE and the optimized locations of actuators selected following the criterion in [20] from the same subsets are shown in figure 13(b) and 13(c) respectively. The corresponding singular-values of the input matrices for the three cases are listed below as: $[S]_a$=diag[0.0615,0.0448, 0.0334,0.0282,0.0218,0.0201],$[S]_b$=diag[0.0617,0.0480,0.0337,0.0287,0.0199,0.0107],$[S]_c$=diag[0.0570,0.0448,0.0339,0.0315,0.0297,0.0185].

It could be easily seen that the minimal singular-value in case (a) has the largest value, and that in case (c) has the second largest value. As demonstrated below, the minimal value of the singular values reflects the capability of control of the design system. To evaluate the

results of the three types of actuator locations in figure 9, the damping ratios are calculated under the condition that with the same feedback gain matrices, [*G*] from (26), to achieve the desired damping ratios 0.35% for all six modes, while the original damping ratios of modes 1-6 is assume 1%. Because of coupling of the residual modes, the actual eigenvalues solved from equation (37) will be shifted away from the desired damping ratio for some controlled modes. Through eigenvalue analysis, the modal damping ratios of mode 1~6 under the three types of actuator locations are listed in table 3. It can be seen from table 3 that almost all the calculated damping ratios are 3.5%, while mode 4 is slightly smaller. Meanwhile, the damping ratios of all the residual modes are positive (not listed here), so the system is stable.

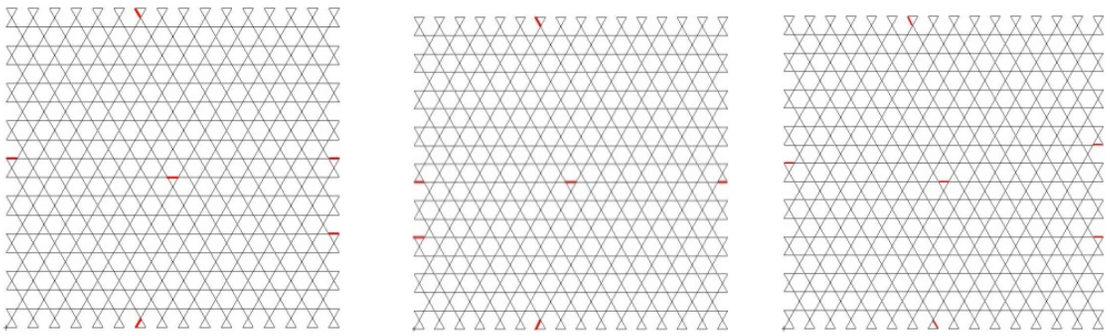

Figure 13. Locations of actuators in the planar Kagome. (a) Optimized by criterion (49). (b) A non-optimal just by using MSE. (c) Optimized by the criterion in [20].

To validate the efficiency of the present optimization method on the actuator placement in reducing physical control forces, the vibration control of the Kagome structure under the excitation of a vertically distributed noise load on the solid face sheet is simulated. The white noise is in a finite bandwidth of 1000Hz. The single-side power spectrum density is $0.3N^2/Hz$.

mode	damping ratio in case(a)	damping ratio in case(b)	damping ratio in case(c)
1	3.5%	3.5%	3.5%
2	3.5%	3.5%	3.5%
3	3.5%	3.5%	3.5%
4	3.45%	3.41%	3.22%
5	3.49%	3.50%	3.49%
6	3.49%	3.49%	3.49%

Table 6. The close-loop modal damping ratios of mode 1~6

The lateral responses of the Kagome structure, observed also at the triangular point shown in figure 2(a), are computed for four cases: without control and with control in the three

types of actuator placements as shown in figure 14. It is found from figure 14(a) that the response amplitudes are considerably reduced through the control by using IMSC method. From the spectra of the responses shown in figure 14(b), the effectiveness of the control method can be more easily seen. The control effect under the three types of actuator locations is almost identical. This is also in agreement with what was demonstrated in table 6 and the finding in [18].

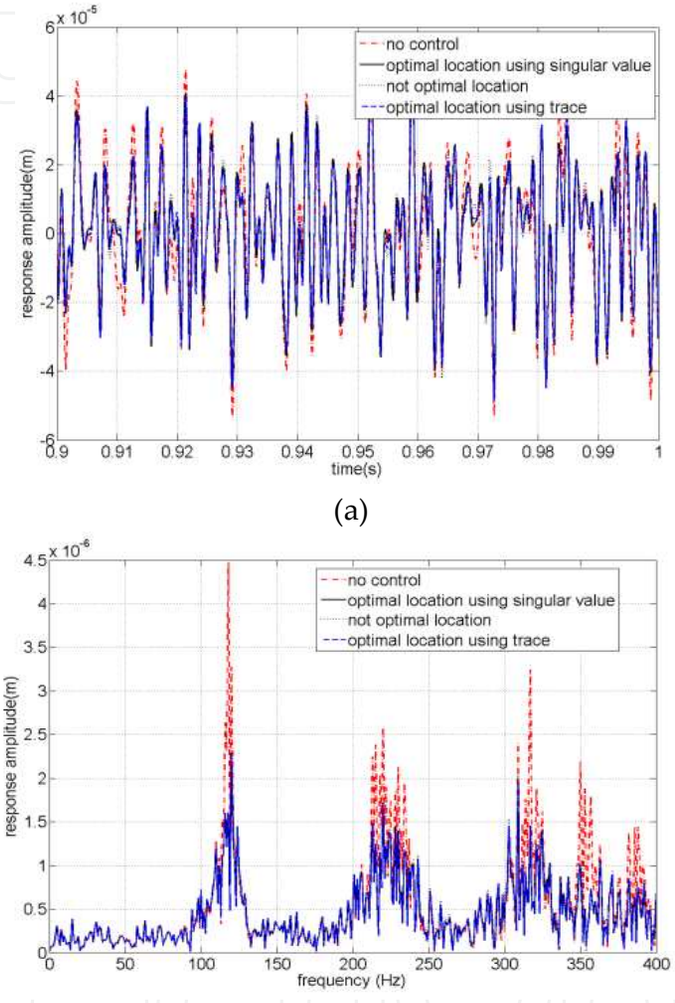

Figure 14. Comparison between uncontrolled and controlled responses under the excitation of white noise. (a) The time history of responses; (b) The spectra of responses.

From the feature of IMSC method, it is known that the main consequence of the types of actuator locations is to cause different requirement on the physical control forces provided by the actuators. To examine the achievement of the present method for the optimal placement of actuators, the root mean square (RMS) values and the maximal instantaneous values of the physical control forces of the six actuators for the three different cases of actuator locations shown in figure 13 are listed in table 7. The physical control forces of the actuator at the same position (the uppermost one) in the three cases are drawn in figure 15.It

is easily seen that the actuator location (c) in figure 13 has a smallest RMS value of the physical forces, that is, an overall least control effort is required. The present optimal method, the actuator location (a) in figure 13, requires a least maximal instantaneous physical control force along with a quite comparable RMS value as that in the actuator location (c). The significant reduction of the maximal actuator force through the optimal placement of actuators has the advantage that the requirement on the capability of actuators is low. From an overall point of view, the present optimal method for the actuator placement with objective function (49) achieves a better result.

case	RMS value (N)	Maximal instantaneous value (N)
(a)	64.17	283.13
(b)	91.04	424.04
(c)	60.39	319.03

Table 7. RMS and maximal instantaneous values of physical forces

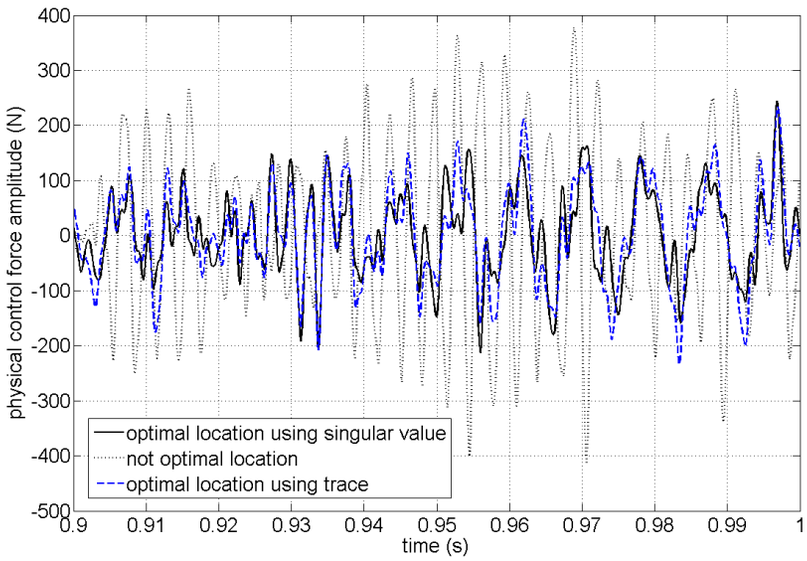

Figure 15. Comparison of the control force in the same actuator.

5. Conclusions

In this chapter, optimization of dampers/actuators placements in the passive/active vibration control of Kagome sandwich structure is studied. In the passive vibration control of Kagome sandwich structure, an optimal placement method of viscoelastic damper for both single mode control and broad-bandwidth control is raised based on FAMSE of the planar Kagome truss. At first, the damper placements for vibration control of mode 1 to mode 3 are carried out and only 0.51% rods in the planar Kagome truss are replaced by dampers in each case. Through complex modal analysis, it is demonstrated that the damping ratios have all gained an increment over 2% which shows the validity

and effectiveness of the present method. For a broad-bandwidth vibration control, a method based on FAMSE is introduced to suppress the vibration in a bandwidth of the first six modes. Only 1.26% rods in the planar Kagome truss are replaced with dampers in this case. The increments of modal damping ratios are over 2% for the modes except for mode 4 and 6, whose increments are 1.41% and 1.86% respectively. Through time-domain simulations under a broad-bandwidth excitation, the reduction of the vibration responses and the spectrum peaks can be seen obviously. It is noticed that when rods in the planar Kagome truss are replaced by the dampers with low-stiffness, the increase of damping factors can be achieved at the cost of losing stiffness of the structure. It is important to get a balance between the increase of damping and the loss of stiffness of the structure.

In the active vibration control of Kagome sandwich structure, a two-step method for the optimal placement of actuators using both modal strain energy and singular value of input matrix is devised. The validity of this method is examined and verified through the eigenvalue analysis and the time-domain simulations. In this part, the stability of system under IMSC with an observer is analyzed and the method to suppress spillover is introduced. It is demonstrated that for the given modal control forces, the maximal physical control force is related to the minimal singular value of the input matrix. Through the optimal placement of actuators, an input matrix with a relatively larger minimal singular value should be realized so that a relatively smaller maximal physical control force is required to achieve the given modal forces. It is also found that MSE, which is widely used to choose the proper locations of dampers/actuators, can not be solely used to get the optimal locations of actuators in IMSC. Due to the influence of the symmetrical features in the Kagome structure and its mode shapes, an inappropriate placement of actuators just according to the magnitudes of MSE may result in the uncontrollability of the structure.

Author details

Kongming Guo and Jun Jiang*
State Key Laboratory for Strength and Vibration, Xi'an Jiaotong University, Xi'an, China

Acknowledgement

The work is supported by the National Fundamental Research Project (973) under the grant No. 2006CB601206.

6. References

[1] Torvik P J, Strickla D Z (1972) Damping additions for plates using constrained viscoelastic layers, Journal of the Acoustical Society of America, 51:985-991.

* Corresponding Author

[2] Ip K H ,Tse P C (2001) Optimal configuration of a piezoelectric patch for vibration control of isotropic rectangular plates, Smart materials and structures. 10: 395-403

[3] Corr L R, Clark W W (2002) Comparison of low-frequency piezoelectric switching shunt techniques for Structural damping, Smart materials and structures. 11:370-376.

[4] Baz A, Ro J (1996) Vibration control of plates with active constrained layer damping, Smart materials and structures. 5:272-280.

[5] dos Santos e Lucato S L, Wang J, Maxwell P, McMeeking R M , Evans A G (2004) Design and demonstration of a high authority shape morphing structure, Int. J. Solids Struct., 41: 3521–3543.

[6] Haftka R T, Adelman H M (1985) Selection of Actuator Locations for Static Shape Control of Large Space Structures by Heuristic Integer Programming, Computers and Structures , 20: 575–582.

[7] Burdisso R A ,Haftka R T (1990) Statistical analysis of static shape control in space structures AIAA Journal, 28:1504-1508.

[8] Chen G S, Bruno R J , Salama M (1991) Optimal placement of active/passive members in truss structures using simulated annealing ,AIAA Journal 29: 1327-1234.

[9] Rao S S , Pan T S , Venkayya V B (1991) Optimal Placement of Actuators in Actively Controlled Structures Using Genetic Algorithms, AIAA Journal, 29: 942–943

[10] Preumont A, Dufour J P , Malekian C (1992) Active damping by a local force feedback with piezoelectric actuators Journal of Guidance, Control and Dynamics 15:390-395

[11] Bilbao A, Avilés R, Aguirrebeitia J , Bustos I F (2009) Eigensensitivity-based optimal damper location in variable geometry trusses AIAA Journal, 47：576-590.

[12] Hutchinson R G , Wicks N, Evans A G , Fleck N A, Hutchinson J W (2003) Kagome plate structures for actuation, Int. J. Solids Struct , 40 :6969–6980.

[13] Guo X, Jiang J (2001) Passive vibration control of truss-cored sandwich plate with planar Kagome truss as one face plane, Science China-Technological Sciences , 54: 1113-1120.

[14] Zhang J, Zheng G T (2007) The Biot Model and Its Application in Viscoelastic Composite Structures, J of Vibration and Acoustics, 129:533-540.

[15] Xu B, Jiang J S (2004) Integrated optimization of structure and control for piezoelectric intelligent trusses with uncertain placement of actuators and sensors, Computational Mechanics 33: 406-412.

[16] Meirovitch L , Baruh H (1981) Optimal control of damped flexible gyroscopic systems, Journal of Guidance and Control, 4:157–163.

[17] Sesak J R, Likins P , Coradetti T (1979) Flexible Spacecraft Control by Model Error Sensitivity Suppression , The Journal of the Astronautical Sciences, 27: 131-156.

[18] Baruh H, Meirovitch.L (1981)On the placement of actuators in the control of distributed-parameter systems AIAA paper 81-0638: 611-619.

[19] Lindberg Jr R E, Longman R W (1984) On the number and placement of actuators for independent modal space control, Journal of Guidance and Control 7: 215-221

[20] Lammering R, Jia J H , Rogers C A (1994) Optimal placement of piezoelectric actuators in adaptive truss structures J.Sound Vib. 171: 67-85

[21] Liu Z S, Wang D J , Hu H C , Yu M (1994) Measures of modal controllability and observability in vibration control of flexible structures Journal of Guidance, Control and Dynamics 17: 1377-1380.

IntechOpen